Title
In Situ X-ray Absorption Spectroscopy Studies of Discharge Reactions in a Thick Cathode of a Lithium Sulfur Battery

Journal
Journal of The Electrochemical Society, 164(2)

ISSN
0013-4651

Authors
Wujcik, Kevin H
Wang, Dunyang Rita
Pascal, Tod A
et al.

Publication Date
2017

DOI
10.1149/2.1441614jes

Peer reviewed

In Situ X-ray Absorption Spectroscopy Studies of Discharge Reactions in a Thick Cathode of a Lithium Sulfur Battery

Kevin H. Wujcik,[a,b] Dunyang Rita Wang,[b,c] Tod A. Pascal,[d] David Prendergast,[d] and Nitash P. Balsara[a,b,e,*,z]

[a]*Department of Chemical and Biomolecular Engineering, University of California, Berkeley, California 94720, USA*
[b]*Materials Sciences Division, Lawrence Berkeley National Laboratory, Berkeley, California 94720, USA*
[c]*Department of Materials Science and Engineering, University of California, Berkeley, California 94720, USA*
[d]*Molecular Foundry, Lawrence Berkeley National Laboratory, Berkeley, California 94720, USA*
[e]*Environmental Energy Technologies Division, Lawrence Berkeley National Laboratory, Berkeley, California 94720, USA*

Lithium sulfur (Li-S) batteries are well known for their high theoretical specific capacities, but are plagued with scientific obstacles that make practical implementation of the technology impossible. The success of Li-S batteries will likely necessitate the use of thick sulfur cathodes that enable high specific energy densities. However, little is known about the fundamental reaction mechanisms and chemical processes that take place in thick cathodes, as most research has focused on studying thinner cathodes that enable high performance. In this work, in situ X-ray absorption spectroscopy at the sulfur K-edge is used to examine the back of a 115 μm thick Li-S cathode during discharge. Our results show that in such systems, where electrochemical reactions between sulfur and lithium are likely to proceed preferentially toward the front of the cathode, lithium polysulfide dianions formed in this region diffuse to the back of the cathode during discharge. We show that high conversion of elemental sulfur is achieved by chemical reactions between elemental sulfur and polysulfide dianions of intermediate chain length (Li_2S_x, $4 \leq x \leq 6$). Our work suggests that controlling the formation and diffusion of intermediate chain length polysulfide dianions is crucial for insuring full utilization of thick sulfur cathodes.

 [DOI: 10.1149/2.1441614jes]

Manuscript submitted September 2, 2016; revised manuscript received November 14, 2016. Published December 1, 2016.

Lithium sulfur batteries have become a widely popular focus of energy storage research due to their high theoretical specific capacity of 1672 mA-h/g.[1,2] The overall reaction mechanism that governs the Li-S discharge processes is given by:

$$S_8 + 16Li^+ + 16e^- \rightarrow 8Li_2S \quad [1]$$

The actual reaction mechanism involves a series of electrochemical reactions with lithium polysulfide reaction intermediates (Li_2S_x, $2 \leq x \leq 8$, referred to as polysulfide dianions; or LiS_x, $3 \leq x \leq 5$, referred to as polysulfide radical anions).[3–8] One example of an electrochemical reaction pathway is:

$$S_{8(s)} + 2Li^+ + 2e^- \rightarrow Li_2S_8 \quad [2]$$

$$3/4\,Li_2S_8 + 1/2Li^+ + 1/2e^- \rightarrow Li_2S_6 \quad [3]$$

$$2/3\,Li_2S_6 + 2/3Li^+ + 2/3\,e^- \rightarrow Li_2S_4 \quad [4]$$

$$1/2\,Li_2S_4 + Li^+ + e^- \rightarrow Li_2S_2 \quad [5]$$

$$1/2\,Li_2S_2 + Li^+ + e^- \rightarrow Li_2S_{(s)} \quad [6]$$

A decrease in the chain length of polysulfides is thus an unambiguous signature of electrochemical reactions. However, polysulfides are also known to undergo chemical reactions, for example:[9]

$$S_8 + 2Li_2S_4 \rightarrow 2Li_2S_8 \quad [7]$$

The evolution of polysulfide chain length in the presence of both electrochemical and chemical reactions is difficult to predict.

Lithium polysulfides tend to dissolve into the electrolyte, resulting in loss of cell capacity. It is thus not surprising that a great deal of research focuses on solving the issues related to polysulfide dissolution.[10–13] Many researchers have recognized that in order for Li-S cells to have high specific energy density and be competitive in cost with current lithium ion battery technology, Li-S cell cathodes must have high area-specific sulfur loadings.[14–16] These high sulfur loadings can only be achieved by making the Li-S cell cathodes thicker. For example, Qie et al. obtained high areal capacities for Li-S cells with thick, pure sulfur cathodes.[17] Hagen and Cheon et al. have shown that increasing cathode thickness leads to significant drops in cell capacity, as additional scientific challenges are introduced.[16,18] Increasing cathode thickness amplifies concentration polarization effects and plating of Li_2S (and possibly Li_2S_2) at the front of the electrode.[18] These problems are magnified if the battery is cycled at high rates of charge and discharge.

Despite their apparent importance, little is known about the chemical and electrochemical reactions that take place in thick sulfur cathodes. The purpose of this paper is to shed light on these reactions. In particular, we focus on chemical/electrochemical processes that take place at the back of thick sulfur cathodes. This is accomplished by in situ X-ray absorption spectroscopy (XAS).

X-ray absorption spectroscopy at the sulfur K-edge has become a popular technique for studying Li-S battery chemistry.[7,19–28] XAS is element-specific and capable of detecting species that are amorphous or crystalline, dilute or concentrated. It also allows researchers to probe Li-S cells without any deconstruction of the cell itself. Interpretation of XAS data from Li-S cells is challenging due to the lack of spectral standards for the polysulfide species.[28–30] However, we have recently shown that the X-ray absorption spectra for lithium polysulfide molecules can be calculated from first principles, thus enabling unambiguous interpretation of experimentally obtained X-ray spectra.[26,31]

In this work, in situ X-ray absorption spectroscopy at the sulfur K-edge is used to examine an Li-S cell cathode during discharge. The low energy of sulfur K-edge X-rays, and the presence of sulfur in the cathode (which absorbs sulfur K-edge X-rays) limited the penetration of X-rays into the cathode. Thus, our data reflects the products of chemical and electrochemical reactions that occur at the back of the thick cathode.

Experimental

Electrolyte preparation.—All electrolyte, cathode, and cell preparation was performed in an argon-filled glove box (MBraun). Electrolyte films were prepared using a diblock copolymer of polystyrene-poly(ethylene oxide) (SEO) purchased from Polymer Source Inc.,

*Electrochemical Society Member.
[z]E-mail: nbalsara@berkeley.edu

having polystyrene and poly(ethylene oxide) molecular weights of 165 kg/mol and 205 kg/mol, respectively. Lithium perchlorate ($LiClO_4$) (Sigma-Aldrich) was dried for 24 hours under vacuum at 90°C before use. SEO and $LiClO_4$ were added to n-methylpyrrolidone (NMP) (EMD Millipore) in an amount equivalent to 11 wt% solids, and allowed to mix overnight at 90°C. The solution was then cast onto nickel foil using a doctor blade and allowed to dry at 60°C overnight. The resulting film was peeled from the nickel foil and dried under vacuum at 90°C overnight. The dry film composition had a $LiClO_4$ amount equivalent to an 'r' value of r = 0.085, where 'r' is the ratio of lithium ions per ethylene oxide monomer.

Cathode preparation.—Cathode slurries contained S_8 (Alfa Aesar), carbon black (Denka), $LiClO_4$, and SEO (identical to that which was used in the electrolyte separator) mixed in NMP, such that the slurry was 15 wt% solids. The slurry was mixed overnight at 90°C and subsequently mixed using a homogenizer (Polytron) set to 15,000 RPM. Homogenization was performed three times, five minutes each time with five minute breaks in between each homogenization to prevent the solution from heating up past undesirable temperatures. The resulting slurry was then poured into a clean Teflon petri dish that was placed on a hot plate at 60°C. The slurry was routinely spread along the bottom of the petri dish using a clean spatula every 30 minutes for 4 hours until the cast slurry was dry enough that it no longer dewet the Teflon surface. The temperature of the hot plate was then set to 50°C and the film was allowed to dry overnight. The film was then peeled from the petri dish and dried overnight under vacuum at 50°C. The dry composition of all cathodes used in the study was 13.0 wt% S_8, 50.7% SEO, 6.2% $LiClO_4$ and 30.0% carbon.

In situ XAS cell.—In situ X-ray absorption spectroscopy was performed using a custom designed cell that enabled X-rays to probe the cathode during charge/discharge. Figure 1a shows the cell schematic along with the corresponding identity for all of its components. Figure 1b shows an image of the in situ cell.

A circular piece of the freestanding cathode film was punched at a diameter of 7/16″. The thickness of the disc was measured using a micrometer, and determined to initially be 130 ± 10 μm. The disc was then placed between two fluorinated ethylene propylene (FEP) sheets and pressed for 30 seconds using a hand press at room temperature. The film thickness was then measured again and determined to be 115 ± 5 μm. An electrolyte disc was then cut from the electrolyte film described above, at a diameter of 9/16″. The cathode disc was then gently pressed to the punched electrolyte disc, placed between two (FEP) sheets and pressed for 30 seconds using a hand press at room temperature. The electrolyte disc used in this experiment had a thickness of 35 μm.

Lithium metal chips (MTI), having a thickness of 250 μm were used as the anode material and were further punched to be 7/16″ in diameter. To assemble the cell, the lithium metal chip was placed on a stainless steel shim (component #4 in Figure 1). The shim had a ring of Kapton tape placed around the edges that had an inner diameter of 8/16″, and an outer diameter equal to the diameter of the shim. This tape ring assured that the lithium metal would stay in place during cell assembly and prevented any unwanted contact between the positive and negative electrodes.

After the lithium was pressed to the stainless steel shim, the electrolyte/cathode assembly was then placed on top of the lithium metal. A circular piece of 55 μm thick aluminum mesh (MTI), punched to a diameter of 7/16″ was then placed on top of the cathode film. This assembly was then placed inside the cell housing as shown in Figure 1. The cell was fastened down to insure contact between the lithium metal, electrolyte separator, cathode, and aluminum mesh interfaces. The O-rings shown in Figure 1a assured that the cell was air-tight. The ultra-thin Kapton film (8 μm thick) (Fralock) allowed X-ray photons to enter and leave the cell while also preventing air exposure of the Li-S cell inside.

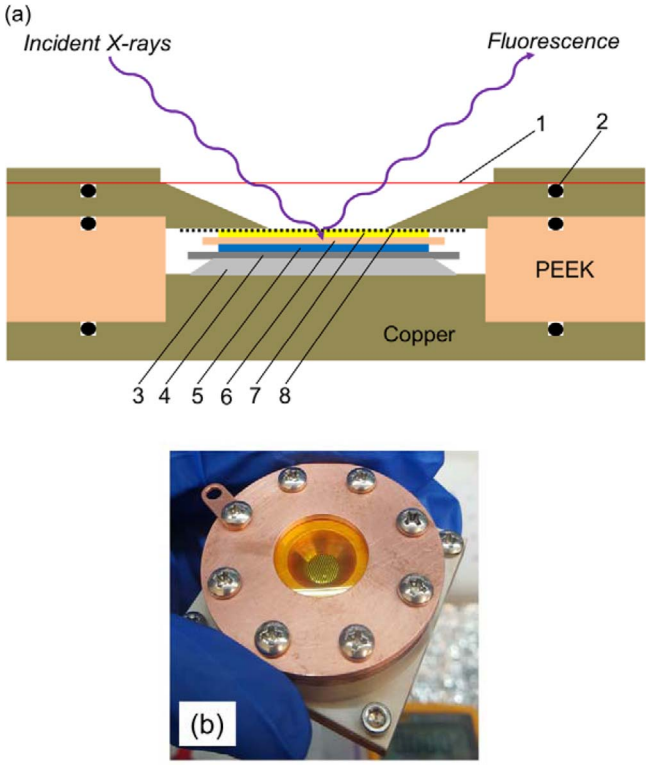

Figure 1. (a) Schematic of cell housing used for in situ XAS experiments: (1) Ultrathin Kapton film (8 μm thick), (2) O-ring, (3) stainless steel spring, (4) stainless steel shim, (5) lithium metal anode, (6) SEO/$LiClO_4$ electrolyte separator, (7) sulfur cathode (elemental sulfur, carbon black, SEO, $LiClO_4$), (8) electronic grade aluminum mesh. (b) Image of in situ XAS cell.

Battery cycling.—The Li-S cell was held at a temperature of 80°C for 8 hours before discharge, and discharged at 80°C while X-rays probed the cathode. Discharge was performed using a VMP3 Potentiostat (Bio-Logic). The cell was discharged at a rate of C/80, calculated using the measured mass of the cathode electrode, the known weight percent of sulfur in the cathode, and assuming a theoretical capacity of 1672 mA-h/g for sulfur. Discharge was stopped at 1.50 V.

Experimental X-ray absorption spectroscopy measurements.—XAS measurements were performed at beamline 4–3 of the Stanford Synchrotron Radiation Lightsource. Preliminary XAS experiments were performed at beamline 9.3.1 of the Advanced Light Source (Lawrence Berkeley National Laboratory). Measurements were taken in fluorescence mode using a four element Vortex detector, with 0.1 eV energy resolution around the absorption K-edge. One scan took roughly 8 minutes to collect, equivalent to roughly 2.75 mA-h/g of capacity was passed per scan. The beam spot size was 5 mm^2 and was not moved during discharge. The Li-S cell was measured in a helium-filled chamber, and was placed on a custom-made heating stage equipped with a PID temperature controller. Calibration of the X-ray energy was performed using sodium thiosulfate (Sigma-Aldrich), setting the first peak maximum to 2472.02 eV.

Data analysis.—Data was normalized and background subtracted using Athena.[32] Least squares fitting of the experimental spectra with the theoretical spectra was performed using a least squares fitting program created by Matthew Marcus at the Advanced Light Source. The theoretical spectra used to analyze the data were those presented by Pascal et al. in a previous publication.[26] In our previous work, least squares fitting of the experimental spectra with theoretical spectra was only performed up to an X-ray energy of 2474.5 eV.[7] This was done, in part, because above ~2473.0 eV, the original theoretical spectra lack absorption intensity compared to the experimental spectra. Obtaining

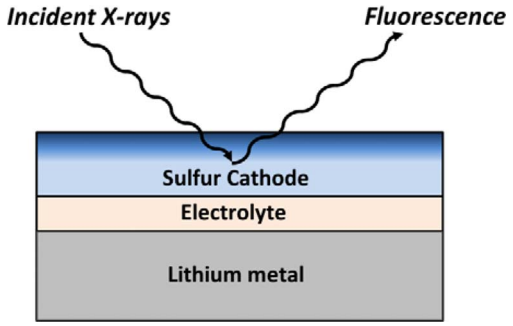

Figure 2. Simplified X-ray absorption spectroscopy experiment schematic. Darkened (upper) region of the cathode represents the thickness that was probed by X-rays.

accurate absorption intensities in this region would require a significant amount of computational resources. To correct for this difference in intensity, and allow fitting of the theoretical and experimental spectra to be performed at all energies, an arctangent step function was added to the theoretical spectra to account for the lack of intensity above the main edge. To determine the parameters of the arctangent function added to the theoretical spectra, an arctangent function was added to the theoretical spectrum of S_8, and its parameters regressed until the theoretical spectrum matched the known experimental spectrum. The arctangent function was centered at 2473.0 eV, had a height of 0.40 (arb. units) and a width of 0.20 eV. We note that because the arctangent step function was centered at 2473.0 eV, its addition has little effect on the main-edge and pre-edge intensities, areas, and ratio.

Results

We begin our analysis by examining the schematic of the cell used for the XAS measurements, shown in Figure 2. The Li-S cell probed in this study consisted of a lithium metal anode, a block copolymer electrolyte separator of SEO with $LiClO_4$, and a cathode that contained elemental sulfur, carbon black, SEO, and $LiClO_4$. X-rays entered the cell through an aluminum mesh current collector on the back of the cathode. The cathode used in this experiment had a thickness of 115 μm. At this thickness, and given that the experiments were carried out at the sulfur K-edge, it is expected that X-ray photons do not probe the entire cathode thickness. To gain an accurate understanding as to what depth of the cathode incident X-rays did probe, the X-ray transmission to a variety of depths within the cathode was calculated using the known cathode composition and atomic absorption coefficients (see Supporting Information for details). The results of these calculations are summarized in Table I, where we report the expected fraction of incident photons that are capable of penetrating to the reported depth in column 2. After incoming photons have taken part in the excitation of a core-shell electron, fluorescent photons, which have a lower energy than incident photons, must then emerge from within the cathode to arrive at the detector. Column 3 of Table I thus represents the fraction of photons emerging from a given depth. The detected signal depends on the product of the fractions given in columns 2 and 3. This enables estimation of the fraction of the XAS signal that can be attributed to each slice through the cathode. This fraction is given in column 4. It is evident from this calculation that the signal is dominated by sulfur species in the back of the cathode, about 30 μm from the current collector. The darkened region of the cathode in Figure 2 represents the portion of the cathode probed in this study.

The Li-S cell was discharged at a constant rate of C/80 based on the sulfur loading. The voltage profile for the discharge process is shown in Figure 3. Here, cell capacity is represented by the variable *Q*. The overall capacity obtained for the cell was 252 mAh/g, which corresponds to 15.1% of the overall theoretical capacity of lithium sulfur batteries. Cheon et al. studied the effect of increasing cathode thickness on discharge capacity:[18] discharge capacities of 78.9%, 62.8%, and 53.1% of the theoretical capacity were obtained as cathode thickness was increased from 15, to 30, to 60 μm, using discharge rates that were roughly C/25, C/50 and C/100, respectively. Extrapolating the results of Cheon, we would expect the 115 μm thick cathode cell probed here to obtain only 22% of the theoretical capacity, which is similar to that which was obtained here.

Table I. Depth of penetration analysis for the Li-S cathode based on the known cathode composition and X-ray absorption coefficients.

Cathode depth (μm)	Fraction of incoming photons transmitted to given depth	Fraction of fluorescent photons emerging out of the cathode from a given depth	Fraction of XAS signal from a given slice
0	0.811	0.628	-
5	0.652	0.442	0.296
10	0.524	0.311	0.209
15	0.422	0.219	0.147
20	0.339	0.154	0.103
25	0.273	0.108	0.073
30	0.219	0.076	0.051
35	0.176	0.054	0.036
40	0.142	0.038	0.025
45	0.114	0.027	0.018
50	0.092	0.019	0.013
75	0.031	0.003	0.025
100	0.010	0.001	0.004
115	0.005	0.000	0.001

The discharge profile reported in Figure 3 is qualitatively similar to that obtained by Cheon et al. in thick cathodes, and contains two regimes (sloping plateaus). Generally, the first plateau announces the formation of soluble polysulfides while the second plateau is taken as a signature of the formation of Li_2S. The extent to which this is true in thick cathodes remains to be established. It is important to note that the second plateau in our cells and the cells used by Cheon et al. is much shorter than that obtained in thin sulfur cathodes. For instance, in a previous study, we examined the discharge performance of an Li-S cell with identical composition to the one studied here, but with a thinner cathode (∼35 um). This cell obtained a first discharge capacity of 661 mAh/g (at a discharge rate of C/40). Cheon et al. suggest that the poor performance of thick Li-S cathodes is due to preferential plating of Li_2S at the front of the cathode, leading to pore blockage. While phenomena that are occurring throughout the entire cathode are outside the scope of our experiment, it is likely that the 115 um

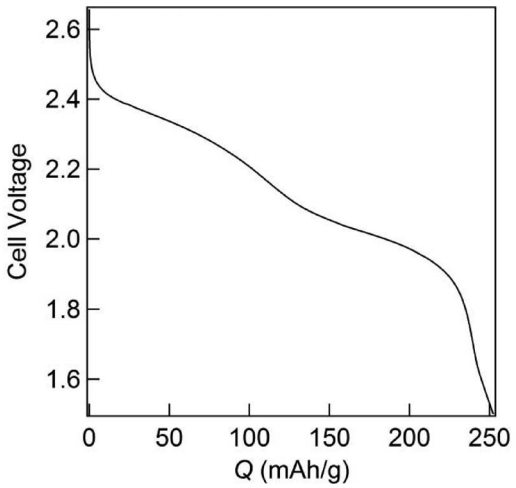

Figure 3. Cell voltage versus capacity (*Q*) obtained for the first discharge of the Li-S cell probed with X-ray's at a constant discharge rate corresponding to C/80.

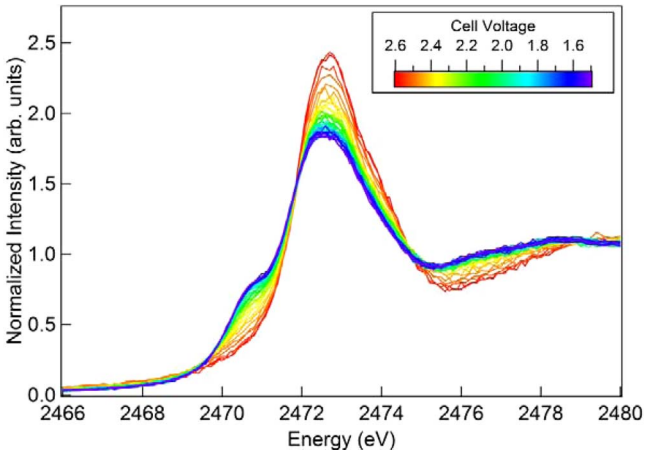

Figure 4. Sulfur K-edge X-ray absorption spectra obtained for the Li-S cell cathode during first discharge.

thick cathode used in this study discharges unevenly. Electrochemical reactions are more likely to occur at the front of the electrode than the back.

Figure 4 shows the sulfur K-edge X-ray absorption spectra obtained throughout discharge. The spectra are characterized by two peaks: one peak at 2472.6 eV, referred to as the main-edge peak due to its occurrence at the expected absorption edge of sulfur, and a second at roughly 2471.0 eV, referred to as the pre-edge peak due to its occurrence being just below the sulfur absorption edge.

X-ray spectra of lithium polysulfides based on first principles calculations given by Pascal et al. are shown in Figure 5a.[26] The X-ray spectra of the reactant and expected final product, S_8 and Li_2S, are shown in Figure 5b. The spectrum of Li_2S is based on first principle calculations; the similarity of the theoretical Li_2S spectrum to the established experimental spectrum for Li_2S validates the methods used to calculate the spectra of lithium polysulfide dianion species.[26] The S_8 spectrum corresponds to that measured before the cell was discharged. (The S_8 spectrum in Figure 5b is qualitatively similar to the theoretical S_8 spectrum given in Reference 26) We use the spectra in Figure 5 to interpret the experimental data presented in Figure 4.

First principles calculations indicate that the pre-edge peak is the signature of X-ray excitations of the charged terminal sulfur ions, while the main-edge peak is related to the uncharged internal sulfur atoms of the polysulfide chain. Therefore, the main-edge to pre-edge peak area ratio reflects the relative population of these sulfur atom types in a given sample, and as such could be regarded as a proxy for the average polysulfide chain length, realizing that a given sample may comprise polysulfide molecules with a distribution of lengths.[26] The relationship between spectral features and average chain length is quantified in Figure 6a. It is evident from simulations of single polysulfide species that polysulfide chain length 'x' of a given polysulfide Li_2S_x is approximately a linear function of the area ratio. The equation corresponding to the least squares fit of the data is given in Figure 6a. We can think of this equation as a calibration for converting the XAS signal into a polysulfide chain length.

The in situ X-ray spectra shown in Figure 4 were fit using two Gaussian peaks (one for the main edge peak and one for the pre-edge peak) and an arctangent function to represent the absorption edge's increase in intensity (see Supporting Information for more details). The resulting ratio of main-edge to pre-edge peak area was calculated for each scan and is shown in Figure 6b as a function of capacity. The expression given in Figure 6a was then used to calculate an approximate average polysulfide chain length, x_{av}. While our calibration expression was developed for single chemical species, we expect it to hold for mixtures because of the fact that we have established the origin of the pre-edge and main-edge features.[26] In principle, the expected value of x_{av} at $t = 0$ is infinity, because lithium is not incorporated into any of the sulfur containing species. Our fitting procedure results in an x_{av} value of 9.72, because the main edge peak of the cathode at $t = 0$ is not perfectly Gaussian. If electrochemical reactions were taking place, then the value of x_{av} determined from XAS would decrease continuously with capacity. This is clearly not the case in Figure 6c. A decrease in x_{av} is detected in the range $0 \leq Q \leq 100$ mAh/g. In contrast, x_{av} is a weak function of capacity in the range $100 \leq Q \leq 252$ mAh/g, suggesting the absence of electrochemical reactions in this regime.

To further elucidate the chemical species formed during discharge, the X-ray spectra were fit using theoretical X-ray absorption spectra given in Figures 5a and 5b.[26] A least squares approach similar to that used in Reference 7 was used to fit the experimental spectra. The composition of the back of the cathode thus obtained is plotted as a function of capacity in Figure 7.

It is evident that no Li_2S is formed at the back of the cathode. Note that the formation of Li_2S is indicated by a peak at 2474.0 eV (Figure 5b). This feature is absent in the XAS spectra from our cell (Figure 4). In other words, the reduction of sulfur at the back of the cathode is far from complete. This is consistent with the findings of Cheon et al.[18]

Figure 7 also shows that spectra were found to consist of a combination of S_8, Li_2S_2, and Li_2S_6. For simplicity, we characterize the polysulfide dianion species using an average chain length for the polysulfide dianions, here referred to as $x_{av_{ps}}$ and calculated as:

$$x_{av_{ps}} = \frac{\left(f_{Li_2S_2} \cdot 2\right) + \left(f_{Li_2S_6} \cdot 6\right)}{f_{Li_2S_2} + f_{Li_2S_6}} \quad [8]$$

Here, $f_{Li_2S_2}$ and $f_{Li_2S_6}$ are the spectral fractions of Li_2S_2 and Li_2S_6 for each experimental spectrum's fit, as shown in Figure 7.

Because the spectra were found to consist of only elemental sulfur and polysulfide dianions, the spectral fraction of sulfur (on an atomic basis) present in the form of polysulfide dianions ($f_{PS,T}$) can then be

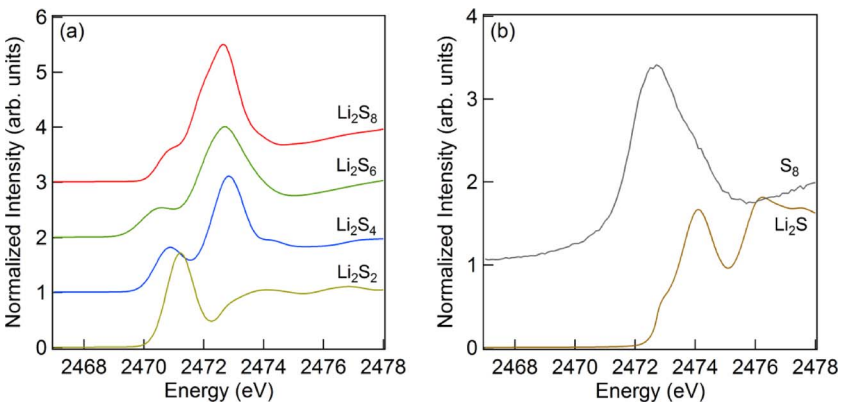

Figure 5. (a) Polysulfide dianion spectral standards, and (b) spectral standards for elemental sulfur and lithium sulfide used to analyze the experimental X-ray spectra.

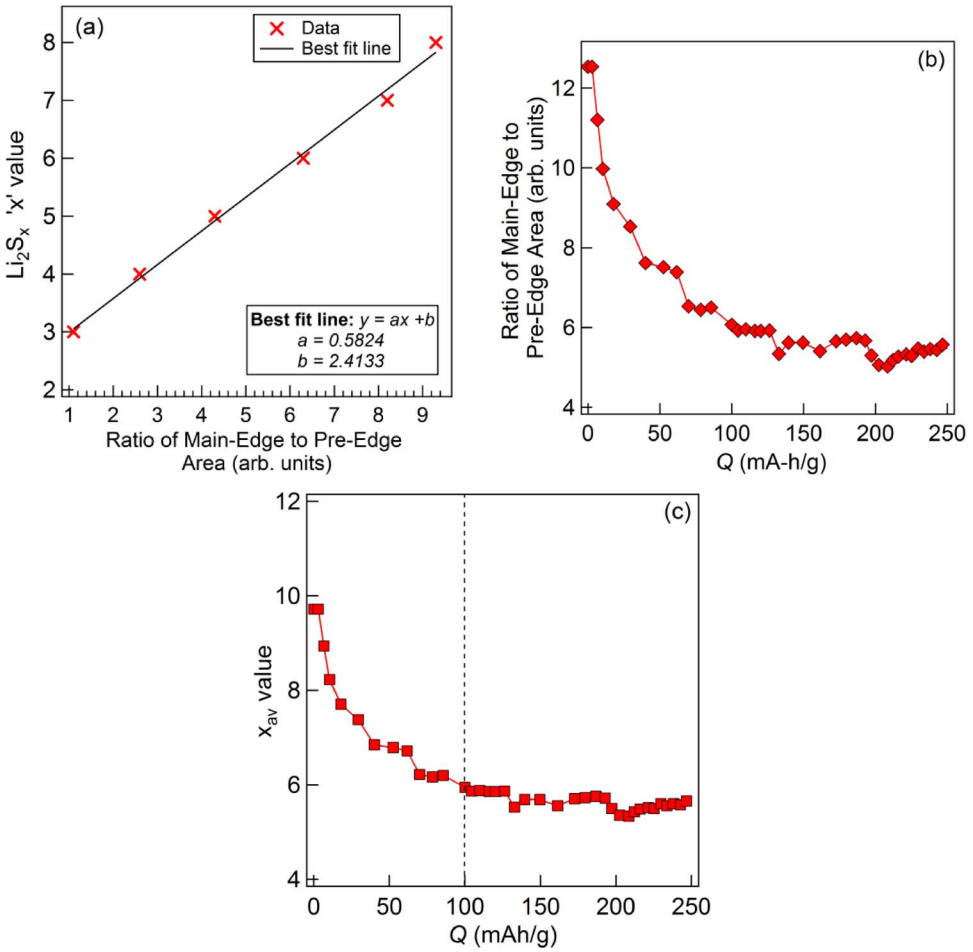

Figure 6. (a) Ratio of main-edge peak area to pre-edge peak area versus corresponding Li_2S_x 'x' value, derived from theoretical spectra as described by Pascal et al.,[26] (b) Ratio of main-edge peak area to pre-edge peak area based on fitting of the experimental spectra shown in Figure 4, (c) Average polysulfide chain length for representing the distribution of polysulfide dianion species present in the cathode as a function of capacity, calculated using the relationship shown in (a) and the ratios shown in (b).

calculated using Equation 9:

$$f_{PS,T} = 1 - f_{S_8} \quad [9]$$

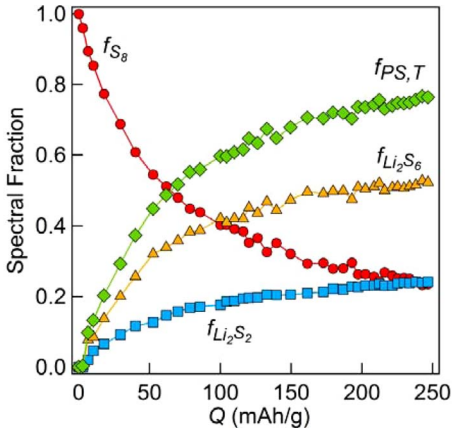

Figure 7. Composition of each in situ spectrum determined by least squares fitting of experimental X-ray spectra with theoretically calculated X-ray spectra as a function of capacity. Here, $f_{PS,T}$ refers to the spectral fraction of polysulfide dianions present, obtained by summing the spectral fractions $f_{Li_2S_2}$ and $f_{Li_2S_6}$, that have an average polysulfide dianion chain length of $x_{av_{ps}}$.

The spectral fraction of polysulfide dianions ($f_{PS,T}$) is also plotted in Figure 7.

With that, the spectra shown in Figure 4 can be represented as a two component mixture of polysulfide dianions having an average chain length of $x_{av_{ps}}$, and present in a spectral fraction represented by $f_{PS,T}$, and elemental sulfur (S_8) represented by the spectral fraction f_{S_8}. The measured signal from a sulfur-containing molecule is proportional to the number of sulfur atoms in the molecule. Thus, the spectral fractions shown in Figure 7 are converted to mole fractions using Equations 10 and 11:

$$y_{S_8} = \frac{\left(f_{S_8}/8\right)}{\left(f_{S_8}/8\right) + \left(f_{PS,T}/x_{av_{ps}}\right)} \quad [10]$$

$$y_{PS,T} = \frac{\left(f_{PS,T}/x_{av_{ps}}\right)}{\left(f_{S_8}/8\right) + \left(f_{PS,T}/x_{av_{ps}}\right)} \quad [11]$$

The mole fractions of S_8 and polysulfide dianions are referred to as y_{S_8} and $y_{PS,T}$, respectively. It is then convenient to determine the amount of lithium that has reacted with sulfur as a function of capacity, which we do in Equation 12:

$$x_{av_{all}} = \frac{y_{S_8} \cdot 8 + y_{PS,T} \cdot x_{av_{ps}}}{y_{PS,T}} \quad [12]$$

Here, $x_{av_{all}}$ represents the expected polysulfide dianion chain length if all of the sulfur were to react with lithium to create a single

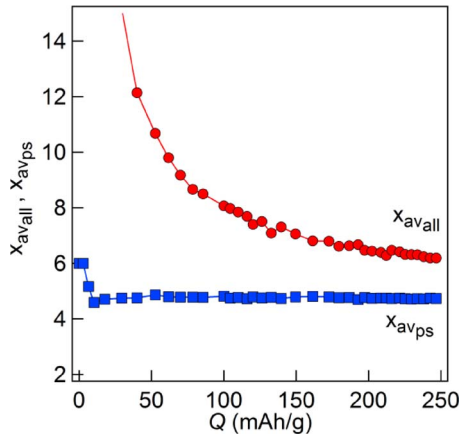

Figure 8. Ratio of lithium to sulfur represented in the stoichiometric form of a polysulfide dianion for the overall system and just the polysulfide dianion species.

polysulfide species with a chain of length $x_{av_{all}}$. The parameter $x_{av_{all}}$ is a hypothetical chain length that would be identical to x_{av} reported in Figure 6c if our analysis were perfect. The estimated chain length of the polysulfide species is $x_{av_{ps}}$. The values of $x_{av_{all}}$, as well as $x_{av_{ps}}$ are plotted as a function of capacity in Figure 8.

Examining Figure 8, we see that the value of $x_{av_{all}}$ drops rapidly at the beginning of discharge, signaling reactions between sulfur and lithium. If reduction were to go to completion, we would expect the value of $x_{av_{all}}$ to decrease at a consistent rate as a function of capacity. Instead, we see that the decrease in $x_{av_{all}}$ slows down, suggesting that transport of lithium to the back of the cathode is limited during later stages of discharge. Interestingly, $x_{av_{ps}}$ remains nearly constant through most of the discharge process.

In principle, polysulfides obtained at the back of the cathode could be either produced by electrochemical reduction of sulfur at the back of the cathode or diffusion of polysulfides produced at the front of the cathode. To distinguish between these possibilities, we examined the total fluorescence intensity reaching the detector during each scan. This intensity is directly proportional to the concentration of sulfur atoms in the back of the cathode that is probed by XAS. For each scan, the fluorescence intensity was averaged over the energy range of 2490–2565 eV, where there are no absorption features. The averaged fluorescence intensity was then normalized by the incoming X-ray intensity measured during each scan. The normalized fluorescence intensity for the zeroth scan (prior to the start of discharge) is called I_0, and the normalized intensity for the 'nth' scan is referred to as I_n. Plotting the ratio of I_n to I_0 as a function of capacity reveals the changes in sulfur content at the back of the cathode through the discharge process. If polysulfides were not diffusing into or out of the back of the cathode then I_n/I_0 would be constant. In Figure 9a we plot I_n/I_0 as a function of capacity. It is evident that I_n/I_0 increases as the cell is discharged. This indicates that polysulfides formed at the front of the cathode are diffusing into the back.

Changes in the sulfur content at the back of the cathode were quantified by noting that:

$$\frac{I_n}{I_0} = \frac{S_T}{S_0} \quad [13]$$

Here, S_0 represents the moles of sulfur atoms in the back of the cathode for the zeroth scan (obtained before discharge began), and S_T is the total moles of sulfur atoms in the back of the cathode for any scan thereafter. The amount of sulfur (on an atomic basis) that has diffused to the back of the cathode can then be determined through Equation 14:

$$S_T - S_0 = S_D \quad [14]$$

Here, S_D represents the amount of sulfur (on an atomic basis) that has diffused to the back of the cathode during discharge. The fraction of sulfur that is present in the back of the cathode as a result of diffusion is given by f_D:

$$\frac{S_D}{S_T} = f_D \quad [15]$$

The fraction of sulfur (on an atomic basis) that corresponds to sulfur originally present in the back of the cathode since the beginning of discharge is then given by f_0:

$$1 - f_D = f_0 \quad [16]$$

At the beginning of discharge, f_0 is equal to 1, because polysulfide diffusion has not begun. As discharge proceeds, f_0 decreases as polysulfide dianions diffuse to the back of the cathode and f_D increases. This is in contrast to most studies on Li-S cells[4,7,13,33] wherein polysulfide diffusion out of the cathode is addressed. The behavior we report has been seen in Li-S cells with thick cathodes and liquid electrolytes like TEGDME that dissolve polysulfides.[18] The values of f_D and f_0 are plotted as a function of capacity in Figure 9b.

As a result of polysulfide diffusion to the back of the cathode, the spectral fraction of polysulfide dianions ($f_{PS,T}$) consists of two components: 1 polysulfide dianions that have diffused into the back of the cathode, and 2 polysulfide dianions that have been created in the back of the cathode. The spectral fraction of polysulfides present in the back of the cathode as a result of diffusion ($f_{PS,D}$) is equal to the spectral fraction of sulfur (on an atomic basis) present in the back of the cathode as a result of diffusion:

$$f_{PS,D} = f_D \quad [17]$$

The spectral fraction of polysulfide dianions created in the back of the cathode ($f_{PS,0}$) is then given by:

$$f_{PS,0} = f_{PS,T} - f_{PS,D} \quad [18]$$

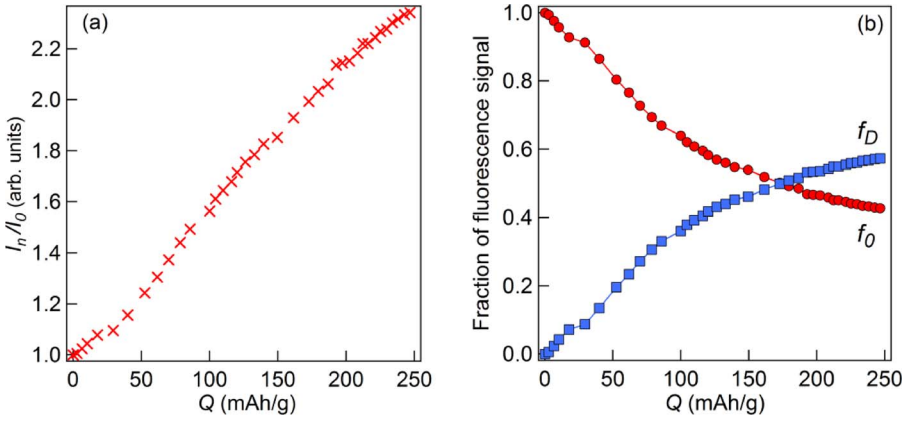

Figure 9. (a) Ratio of fluorescence intensity to initial fluorescence intensity measured before discharge as a function of capacity (I_n/I_0); (b) fraction of fluorescence signal pertaining to sulfur in the back of the cathode since the beginning of discharge (f_0) and fraction of sulfur diffused to the back of the cathode during discharge (f_D).

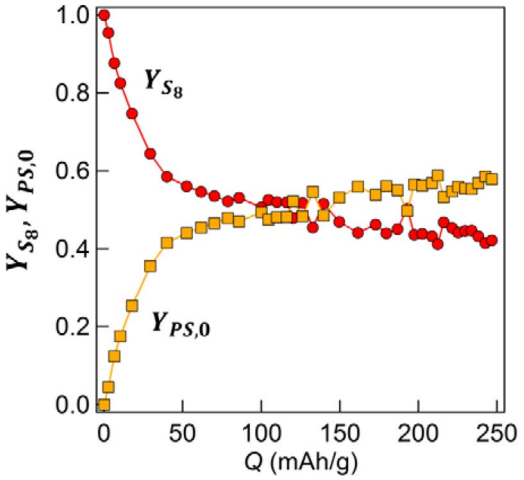

Figure 10. The fraction of sulfur (on an atomic basis) originally in the back of the cathode at the beginning of discharge proportioned into two components: unreacted elemental sulfur, having a mole fraction of Y_{S_8} and polysulfide dianions, having a mole fraction of $Y_{PS,0}$.

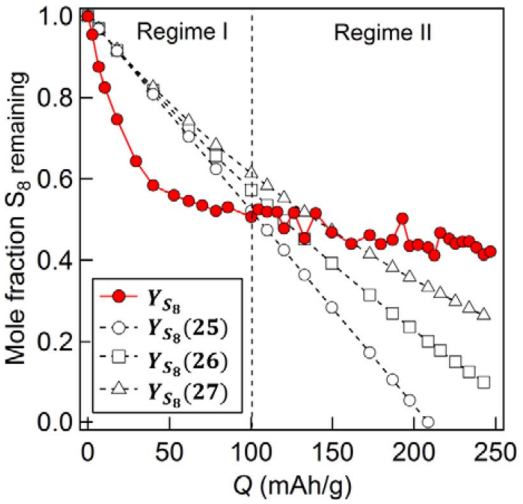

Figure 11. Mole fraction of elemental sulfur remaining based on the spectroscopic analysis (filled symbols) and three assumed hypothetical electrochemical reduction Reactions 25, 26, and 27 (open symbols).

The overall mole fraction of polysulfide dianions, $y_{PS,T}$, thus consists of a mole fraction of diffused polysulfide dianions ($y_{PS,D}$), and a mole fraction of polysulfide dianions created in the back of the cathode ($y_{PS,0}$), calculated through Equations 19 and 20, respectively:

$$y_{PS,D} = \frac{\left(f_{PS,D} \,/_{x_{av_{ps}}}\right)}{\left(f_{S_8}/8\right) + \left(f_{PS,T} \,/_{x_{av_{ps}}}\right)} \quad [19]$$

$$y_{PS,0} = \frac{\left(f_{PS,0} \,/_{x_{av_{ps}}}\right)}{\left(f_{S_8}/8\right) + \left(f_{PS,T} \,/_{x_{av_{ps}}}\right)} \quad [20]$$

A second implication of the results shown in Figures 9a and 9b is that the measured fractions of elemental sulfur (f_{S_8} and y_{S_8}) are affected by diffusion of polysulfides from the front of the cathode. In order to determine the true spectral fraction of elemental sulfur in the back of the cathode that was unreacted, we can calculate a corrected spectral fraction of elemental sulfur (referred to as F_{S_8}) through Equation 21:

$$\frac{f_{S_8}}{f_0} = F_{S_8} \quad [21]$$

The dependence of F_{S_8} on capacity is obtained from the dependences of f_{S_8} and f_0 on capacity (Figures 7 and 9b). By definition, the corrected spectral fraction of polysulfides created in the back of the cathode is given by:

$$1 - F_{S_8} = F_{PS,0} \quad [22]$$

The true mole fractions of elemental sulfur and polysulfide dianions for the sulfur in the back of the cathode, Y_{S_8} and $Y_{PS,0}$, are then obtained by using Equations 23 and 24 to convert spectral fractions into mole fractions:

$$Y_{S_8} = \frac{\left(F_{S_8}/8\right)}{\left(F_{S_8}/8\right) + \left(F_{PS,0}/_{x_{av_{ps}}}\right)} \quad [23]$$

$$Y_{PS,0} = \frac{\left(F_{PS,0} \,/_{x_{av_{ps}}}\right)}{\left(F_{S_8}/8\right) + \left(F_{PS,0}/_{x_{av_{ps}}}\right)} \quad [24]$$

The dependence of Y_{S_8} and $Y_{PS,0}$ on capacity is shown in Figure 10. It is evident from this figure that 58% of S_8 is converted to polysulfides at the back of the cathode. Note that in Equations 8 through 24 all quantities are functions of capacity, Q, (or scan number) except I_0 and S_0. For simplicity, this is not explicitly indicated in the equations.

We can then examine how the fraction of elemental sulfur remaining in the back of the cathode compares to what is expected assuming three highly simplified electrochemical reactions:

$$S_8 + 2e^- + 2Li^+ \rightarrow Li_2S_8 \quad [25]$$

$$S_8 + 8/3e^- + 8/3Li^+ \rightarrow 3/4Li_2S_6 \quad [26]$$

$$S_8 + 4e^- + 4Li^+ \rightarrow Li_2S_4 \quad [27]$$

The fraction of sulfur remaining for each hypothetical reaction is calculated using the known number of electrons per sulfur molecule based on the discharge current and known cathode composition. The calculated mole fractions of S_8 remaining for reaction Equations 25, 26, and 27, represented by $Y_{S_8}(25)$, $Y_{S_8}(26)$, and $Y_{S_8}(27)$, respectively, are plotted as a function of capacity in Figure 11, along with the measured mole fraction of elemental sulfur remaining in the back of the cathode.

Figure 11 shows that the fraction of elemental sulfur remaining in the cathode decreases more rapidly than the three assumed electrochemical reactions would allow. This indicates that elemental sulfur cannot be consumed by electrochemical reactions alone. In other words, elemental sulfur at the back of the cathode is consumed both electrochemically and chemically. This mode of elemental sulfur consumption continues until Q = 100 mAh/g, and we refer to this as Regime I. Beyond this point, elemental sulfur consumption is much slower than that expected based on electrochemical reactions. We conclude that sulfur consumption in this regime (Regime II) is dominated by chemical reactions. The crossover from Regime I to Regime II is coincident with the crossover in the voltage profile from the low capacity plateau to the high capacity plateau.

We interpret these results at follows: in Regime I, a combination of chemical and electrochemical reactions result in a systematic decrease of x_{av} at the back of the cathode. At the end of this regime, polysulfides with $x_{av_{ps}}$ of about 5 are obtained, and about 50% of the sulfur at the back of the cathode is consumed. This is followed by Regime II, wherein elemental sulfur is only consumed by chemical reactions. About 58% of the elemental sulfur is consumed at the end of Regime II. Polysulfides with an $x_{av_{ps}}$ of about 5, formed in the front of the cathode, diffuse into the back throughout both regimes, resulting in a dilution of the signal from the elemental sulfur. The slowing down of electrochemical reactions in Regime II may arise due to pore blockage in the front of the electrode and concomitant absence of lithium salt at the back of the cathode or, the coating of

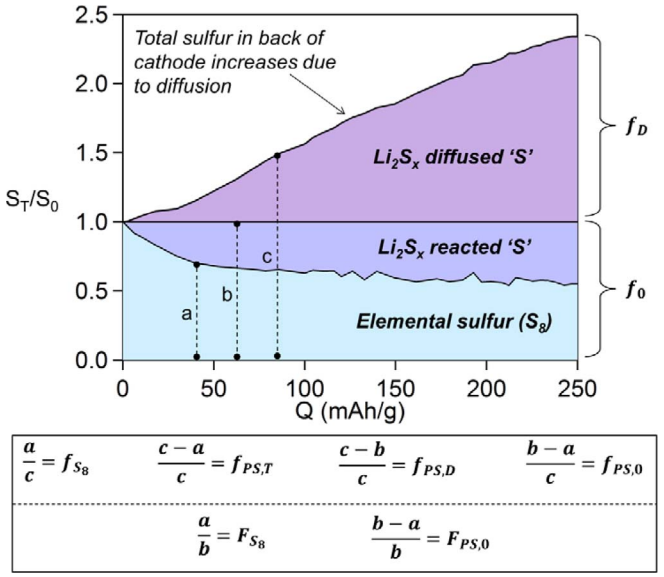

Figure 12. Spectral fractions of elemental sulfur and polysulfide dianions in the back of the cathode as a function of capacity. Here, the lines 'a', 'b', and 'c' are provided along with equations below the plot to graphically illustrate how each variable was calculated. The spectral fractions f_{S_8}, $f_{PS,T}$, $f_{PS,D}$, and $f_{PS,0}$ describe the composition of the back of the cathode as a function of capacity. The variable f_0 represents the fraction of sulfur in the back of the cathode that was present since the beginning of discharge; f_D represents the fraction of sulfur present in the back of the cathode as a result of polysulfide dianion diffusion. The corrected spectral fractions F_{S_8} and $F_{PS,0}$ represent the composition of the sulfur (on an atomic basis) that was present in the back of the cathode since the beginning of discharge.

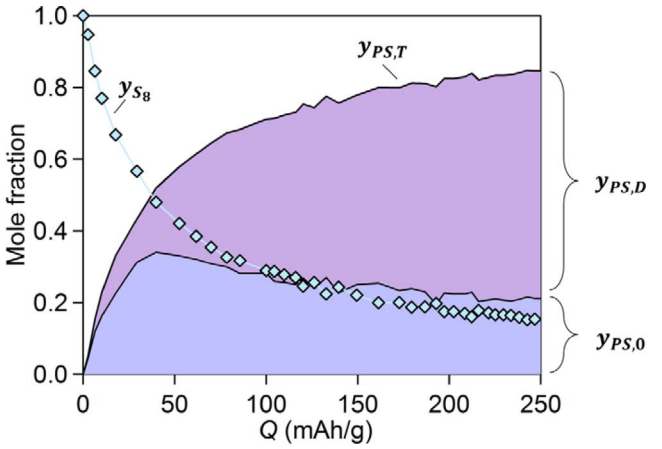

Figure 13. Mole fractions of elemental sulfur (S_8) (y_{S_8}) and polysulfide dianions ($y_{PS,T}$) in the back of the cathode as a function of capacity. The polysulfide dianions in the back of the cathode are split into two components: a mole fraction representing polysulfide dianions that have diffused to the back of the cathode ($y_{PS,D}$) and a mole fraction representing polysulfide dianions created in the back of the cathode ($y_{PS,0}$).

the electronically conducting carbon particles by an insulating precipitate of Li_2S_2 around the electronically conducting carbon particles (see Figure 7).

The nature of chemical reactions occurring in the cathode is not entirely clear. Examining the identity of the polysulfide dianion species (Figure 8) that were present in the cathode, it is also apparent that the chemical consumption of elemental sulfur is coupled to the presence of intermediate chain length polysulfide dianions (Li_2S_x, $4 \leq x \leq 6$). Reactions between elemental sulfur and polysulfide dianions are governed by the following general equation:

$$S_8 + yLi_2S_x \rightarrow yLi_2S_{[x+(8/y)]} \quad [28]$$

Assuming that Li_2S_8 is the longest polysulfide that can be formed, the polysulfide dianion reactant in Equation 28 cannot be Li_2S_8. If the reactant were Li_2S_6, the lowest value of y would be $y = 4$. For shorter chain polysulfides, such as Li_2S_4, $y = 2$. The likelihood that a reaction requiring five reactant molecules would take place (i.e. when Li_2S_6 is the reactant) is lower than that requiring three or fewer molecules. We thus propose that chemical reactions between elemental sulfur and polysulfide dianions likely involve short chain polysulfide dianions (i.e. when Li_2S_2, Li_2S_3, or Li_2S_4 are the reactants), such as:

$$S_8 + 2Li_2S_4 \rightarrow Li_2S_8 \quad [29]$$

Our observation that $x_{av_{ps}}$ remains constant in Regimes I and II indicates that a decrease in polysulfide chain length due to electrochemical reactions is compensated for by an increase in chain length due to chemical reactions, e.g. Reaction 29.

To summarize our overall findings, we present Figure 12, which plots the ratio of total sulfur in the back of the cathode (on an atomic basis) (S_T) to the original amount of sulfur in the back of the cathode (on an atomic basis) (S_0). This ratio is equal to the measured ratio I_n/I_0 presented in Figure 9a. The back of the cathode consists of three components: elemental sulfur, polysulfide dianions that were created in the back of the cathode by electrochemical conversion of sulfur, and polysulfide dianions that diffused to the back of the cathode. The lengths 'a', 'b', and 'c' are used along with equations presented below the plot in Figure 12 to illustrate how the different spectral fractions of each component were calculated. Without the diffusion of polysulfide dianion species, the composition of the back of the cathode could be described by only F_{S_8} and $F_{PS,0}$. However, because polysulfide dianion species diffused to the back of the cathode, the spectral fractions F_{S_8} and $F_{PS,0}$ are effectively diluted, resulting in the spectral fractions f_{S_8}, and $f_{PS,0}$. The spectral fraction of diffused polysulfide dianion species is given by $f_{PS,D}$, which is equal to the fraction of sulfur (on an atomic basis) that has diffused to the back of the cathode (f_D). The spectral fractions f_{S_8}, $f_{PS,0}$, and $f_{PS,D}$ describe the spectra shown in Figure 4.

Converting the spectral fractions of elemental sulfur and polysulfide dianion species to mole fractions, we arrive at Figure 13. Here, we plot the mole fractions of elemental sulfur (y_{S_8}) and all polysulfide dianions ($y_{PS,T}$) in the back of the cathode as a function of capacity. The total mole fraction of polysulfide dianions ($y_{PS,T}$) consists of two components, diffused polysulfide dianions ($y_{PS,D}$), and polysulfide dianions created in the back of the cathode ($y_{PS,0}$). Figure 13 describes the mole fraction of all sulfur containing species in the back of the cathode, whereas Figures 10 and 11 only describe the composition of sulfur (on an atomic basis) that was present in the back of the cathode since the beginning of discharge.

In Figure 13, it is evident that the electrochemical conversion of sulfur into polysulfides dominates the back of the cathode for $0 \leq Q \leq 50$. Beyond this point, electrochemical conversion of elemental sulfur slows down, and diffusion of polysulfides from the front of the cathode becomes increasingly important. In the $Q \geq 100$ mAh/g regime, electrochemical conversion of sulfur is negligible and polysulfide buildup in the back of the cathode is dominated by diffusion from the front. Diffusion of new polysulfide dianions from the front of the cathode slows down as Q approaches 252 mAh/g, because as this point is reached, electrochemical reactions throughout the cathode slow down.

It is perhaps appropriate to conclude this section by highlighting the differences between the approach used in the present study and work we have previously reported.[7] In Reference 7, our group studied the first discharge of an Li-S cell using an X-ray beam that was incident on the lithium side (anode side). The XAS data in this study was thus dominated by polysulfides that were present in the electrolyte separator, rather than the cathode. An important conclusion of the work in Reference 7 was that polysulfide radical anions were detected in the electrolyte due to the presence of an XAS signal at 2468–2469 eV. Signatures of polysulfide radicals were not detected in our

experiments reported in this paper. The formation of radical anions likely occurs through disproportionation reactions with electrochemically formed polysulfide dianions as reactants.[6,7,34] We have also recently shown that in ether based solvents, polysulfide radical anion formation is favored at low concentrations of sulfur.[34] Thus, it is likely that the low concentration of polysulfide species in the electrolyte separator in Reference 7 enabled the formation of polysulfide radical anions. Additionally, the sulfur cathode used in Reference 7 was only 35 um thick. The roles of differences in cathode geometry and the presence of lithium metal in the vicinity of the portion of the cell that was probed by XAS are not clear at this juncture. In the future, we will examine Li-S cells with thick cathodes from the anode side.

In References 9,19–24, in situ XAS was similarly used to probe the Li-S cell cathode, but different results were obtained than those shown here. For instance, Cuisiner et al. detected radical polysulfide anions when dimethylacetamide was used as the solvent.[23] It is well-known that this solvent stabilizes significant concentrations of polysulfide radical anions. Additional differences in the results shown here and the results reported by other in situ XAS studies of Li-S cathodes may stem from: (1) differences in cathode thickness, sulfur loading, or discharge rate (2) the use of low molecular weight solvents rather than the high molecular weight polymer electrolyte used here, and (3) differences in spectral standards and analysis than those presented here. We mention in passing that in a previous study, our group used principle component analysis (PCA) to determine the presence of polysulfide species in chemically synthesized systems.[28] In this case, the data were consistent with the presence of either one or two major components. The present study suggests that the complexity of species formed in a sulfur cathode precludes the use of PCA to determine the presence of particular polysulfide species. Our analysis in this paper is thus restricted to determination of the average length of the polysulfides. Reconciliation of results obtained in different Li-S cells and chemically synthesized polysulfides is a worthwhile but challenging goal that is well beyond the scope of the present study.

Conclusions

In situ X-ray absorption spectroscopy at the sulfur K-edge was used to probe the back of a thick Li-S cathode during discharge. The experimentally obtained spectra were interpreted using theoretical spectral standards. Analysis of the spectra and the fluorescence intensity measured during each scan showed that polysulfide dianion species produced by electrochemical reactions diffused to the back of the cathode during discharge. To our knowledge, this is the first time this phenomenon has been quantified. We explain this finding as follows: the limited diffusion of lithium ions to the back of a thick Li-S cathode will lead to higher reaction rates in the front of the cathode relative to the back of the cathode. This difference in reaction rate leads to a higher concentration of polysulfide dianions in the front of the cathode, which in turn creates a concentration gradient that leads to the diffusion of polysulfide dianions to the back of the cathode.

The conversion of sulfur in the back of the cathode occurs in two distinct steps. In the first step, elemental sulfur is consumed by a combination of electrochemical reduction and chemical reactions. In the second step, elemental sulfur is consumed by chemical reactions alone. Although the capacity obtained for the Li-S cell was low (only 15% of the Li-S cell theoretical capacity), 58% of the elemental sulfur in the back of the cathode was converted to polysulfide dianion species due to a combination of electrochemical and chemical reactions. This result has important implications for our understanding of how Li-S redox reactions proceed, and also when considering the shelf life of partially discharged Li-S cells.

Going further, our results suggest that intermediate chain polysulfide dianions (Li_2S_x, $4 \leq x \leq 6$) are the dominant species at the back of the cathode. Since elemental sulfur is a crystalline insulating solid, it is likely that reactions between elemental sulfur and these intermediate chain length polysulfide dianions are essential for complete utilization of a sulfur cathode.

Our study is but one step toward the complete understanding of processes that occur during the first discharge in an Li-S cell with a thick sulfur electrode.

Acknowledgments

This work was supported by the Assistant Secretary for Energy Efficiency and Renewable Energy, Office of Vehicle Technologies of the US Department of Energy under Contract DE-AC02-05CH11231 under the Battery Materials Research program. Use of the Stanford Synchrotron Radiation Lightsource, SLAC National Accelerator Laboratory, is supported by the U.S. Department of Energy, Office of Science, Office of Basic Energy Sciences under Contract No. DE-AC02-76SF00515. The Advanced Light Source is supported by the Director, Office of Science, Office of Basic Energy Sciences, of the U. S. Department of Energy under Contract No. DE-AC02-05CH11231. We also acknowledge the help of Erik Nelson and Matthew Latimer of SSRL, and Ethan Crumlin and Wayne Stolte of ALS.

List of Symbols

F_{S_8}	Corrected/undiluted spectral fraction of elemental sulfur in the back of the cathode
$F_{PS,0}$	Corrected/undiluted spectral fraction of polysulfide dianions in the back of the cathode
$f_{Li_2S_2}$	Spectral fraction of Li_2S_2 determined through least squares fitting of the experimental spectra with theoretical spectra
$f_{Li_2S_6}$	Spectral fraction of Li_2S_6 determined through least squares fitting of the experimental spectra with theoretical spectra
$f_{PS,T}$	Spectral fraction of polysulfide dianion species in the back of the cathode
f_{S_8}	Spectral fraction of elemental sulfur in the back of the cathode
f_D	Fraction of sulfur (on an atomic basis) in the back of the cathode as a result of diffusion
f_0	Fraction of sulfur (on an atomic basis) in the back of the cathode since the beginning of discharge
I_0	Normalized fluorescence intensity for the zeroth scan
I_n	Normalized fluorescence intensity for the 'nth' scan
Q	Cell capacity
S_T	Total moles of sulfur (on an atomic basis) in the back of the cathode
S_0	Total moles of sulfur (on an atomic basis) in the back of the cathode at the beginning of discharge
S_D	Total moles of sulfur (on an atomic basis) that have diffused from the front of the cathode to the back of the cathode
x_{av}	Average polysulfide dianion chain length for all sulfur containing species in the back of the cathode, calculated using the peak area ratios
$x_{av_{all}}$	Average polysulfide dianion chain length accounting for all sulfur containing species in the back of the cathode
$x_{av_{ps}}$	Average polysulfide dianion chain length for polysulfide dianion species in the back of the cathode
Y_{S_8}	Corrected/undiluted mole fraction of elemental sulfur in the back of the cathode
$Y_{PS,0}$	Corrected/undiluted mole fraction of polysulfide dianions in the back of the cathode
$Y_{S_8}(25)$	Calculated mole fraction of elemental sulfur that would remain assuming the hypothetical reaction shown in Equation 25
$Y_{S_8}(26)$	Calculated mole fraction of elemental sulfur that would remain assuming the hypothetical reaction shown in Equation 26

$Y_{S_8}(27)$ Calculated mole fraction of elemental sulfur that would remain assuming the hypothetical reaction shown in Equation 27

$y_{PS,T}$ Mole fraction of polysulfide dianion species in the back of the cathode

y_{S_8} Mole fraction of elemental sulfur in the back of the cathode

$y_{PS,D}$ Mole fraction of polysulfide dianions in the back of the cathode as a result of diffusion

$y_{PS,0}$ Mole fraction of polysulfide dianions in the back of the cathode that were created in the back of the cathode

References

1. D. Bresser, S. Passerini, and B. Scrosati, *Chemical Communications*, **49**, 10545 (2013).
2. P. G. Bruce, S. A. Freunberger, L. J. Hardwick, and J.-M. Tarascon, *Nature materials*, **11**, 19 (2012).
3. R. D. Rauh, F. S. Shuker, J. M. Marston, and S. B. Brummer, *Journal of Inorganic and Nuclear Chemistry*, **39**, 1761 (1977).
4. C. Barchasz, F. Molton, C. Duboc, J. C. Lepretre, S. Patoux, and F. Alloin, *Analytical chemistry*, **84**, 3973 (2012).
5. N. A. Cañas, D. N. Fronczek, N. Wagner, A. Latz, and K. A. Friedrich, *The Journal of Physical Chemistry C*, **118**, 12106 (2014).
6. Q. Wang, J. Zheng, E. Walter, H. Pan, D. Lv, P. Zuo, H. Chen, Z. D. Deng, B. Y. Liaw, X. Yu, X. Yang, J.-G. Zhang, J. Liu, and J. Xiao, *Journal of The Electrochemical Society*, **162**, A474 (2015).
7. K. H. Wujcik, T. A. Pascal, C. D. Pemmaraju, D. Devaux, W. C. Stolte, N. P. Balsara, and D. Prendergast, *Advanced Energy Materials*, **5** (2015).
8. H. Yamin, A. Gorenshtein, J. Penciner, Y. Sternberg, and E. Peled, *Journal of The Electrochemical Society*, **135**, 1045 (1988).
9. Y. Gorlin, M. U. Patel, A. Freiberg, Q. He, M. Piana, M. Tromp, and H. A. Gasteiger, *Journal of The Electrochemical Society*, **163**, A930 (2016).
10. A. Rosenman, E. Markevich, G. Salitra, D. Aurbach, A. Garsuch, and F. F. Chesneau, *Advanced Energy Materials*, **5** (2015).
11. X. Ji, K. T. Lee, and L. F. Nazar, *Nature materials*, **8**, 500 (2009).
12. X. Ji and L. F. Nazar, *Journal of Materials Chemistry*, **20**, 9821 (2010).
13. A. Manthiram, Y. Fu, and Y.-S. Su, *Accounts of Chemical Research*, **46**, 1125 (2012).
14. D. Eroglu, K. R. Zavadil, and K. G. Gallagher, *Journal of The Electrochemical Society*, **162**, A982 (2015).
15. M. Hagen, S. Dörfler, P. Fanz, T. Berger, R. Speck, J. Tübke, H. Althues, M. J. Hoffmann, C. Scherr, and S. Kaskel, *Journal of Power Sources*, **224**, 260 (2013).
16. M. Hagen, P. Fanz, and J. Tübke, *Journal of Power Sources*, **264**, 30 (2014).
17. L. Qie and A. Manthiram, *ACS Energy Letters*, **1**, 46 (2016).
18. S.-E. Cheon, K.-S. Ko, J.-H. Cho, S.-W. Kim, E.-Y. Chin, and H.-T. Kim, *Journal of The Electrochemical Society*, **150**, A800 (2003).
19. M. A. Lowe, J. Gao, and H. D. Abruna, *RSC Advances*, **4**, 18347 (2014).
20. Y. Gorlin, A. Siebel, M. Piana, T. Huthwelker, H. Jha, G. Monsch, F. Kraus, H. A. Gasteiger, and M. Tromp, *Journal of The Electrochemical Society*, **162**, A1146 (2015).
21. M. Cuisinier, P. E. Cabelguen, B. D. Adams, A. Garsuch, M. Balasubramanian, and L. F. Nazar, *Energy & Environmental Science*, **7**, 2697 (2014).
22. M. Cuisinier, P.-E. Cabelguen, S. Evers, G. He, M. Kolbeck, A. Garsuch, T. Bolin, M. Balasubramanian, and L. F. Nazar, *The Journal of Physical Chemistry Letters*, **4**, 3227 (2013).
23. M. Cuisinier, C. Hart, M. Balasubramanian, A. Garsuch, and L. F. Nazar, *Advanced Energy Materials*, **5**, 1401801 (2015).
24. M. U. M. Patel, I. Arčon, G. Aquilanti, L. Stievano, G. Mali, and R. Dominko, *ChemPhysChem* (2014).
25. X. Feng, M.-K. Song, W. C. Stolte, D. Gardenghi, D. Zhang, X. Sun, J. Zhu, E. J. Cairns, and J. Guo, *Physical Chemistry Chemical Physics*, **16**, 16931 (2014).
26. T. A. Pascal, K. H. Wujcik, J. Velasco-Velez, C. Wu, A. A. Teran, M. Kapilashrami, J. Cabana, J. Guo, M. Salmeron, N. Balsara, and D. Prendergast, *The Journal of Physical Chemistry Letters*, **5**, 1547 (2014).
27. M. Vijayakumar, N. Govind, E. Walter, S. D. Burton, A. Shukla, A. Devaraj, J. Xiao, J. Liu, C. Wang, A. Karim, and S. Thevuthasan, *Physical Chemistry Chemical Physics*, **16**, 10923 (2014).
28. K. H. Wujcik, J. Velasco-Velez, C. H. Wu, T. Pascal, A. A. Teran, M. A. Marcus, J. Cabana, J. Guo, D. Prendergast, M. Salmeron, and N. P. Balsara, *Journal of The Electrochemical Society*, **161**, A1100 (2014).
29. A. Kamyshny, I. Ekeltchik, J. Gun, and O. Lev, *Analytical chemistry*, **78**, 2631 (2006).
30. R. Steudel, *Elemental Sulfur and Sulfur-Rich Compounds II*, Springer Berlin Heidelberg (2003).
31. T. A. Pascal, C. D. Pemmaraju, and D. Prendergast, *Physical Chemistry Chemical Physics*, **17**, 7743 (2015).
32. B. Ravel and M. Newville, *Journal of Synchrotron Radiation*, **12**, 537 (2005).
33. Y. V. Mikhaylik and J. R. Akridge, *Journal of The Electrochemical Society*, **151**, A1969 (2004).
34. K. H. Wujcik, D. R. Wang, A. Raghunathan, M. Drake, T. A. Pascal, D. Prendergast, and N. P. Balsara, *The Journal of Physical Chemistry C*, **120**, 18403 (2016).